Kinetic and Crystallographic Analysis of Active Site Mutants of Escherichia coli γ-Aminobutyrate Aminotransferase †

7 AUTHORS, INCLUDING:

James A Langston
Novozymes
11 PUBLICATIONS   445 CITATIONS

SEE PROFILE

Xianzhi Zhou
Novavax
24 PUBLICATIONS   348 CITATIONS

SEE PROFILE

Andrew Fisher
University of California, Davis
77 PUBLICATIONS   2,567 CITATIONS

SEE PROFILE

Michael D Toney
University of California, Davis
99 PUBLICATIONS   3,538 CITATIONS

SEE PROFILE

Kinetic and Crystallographic Analysis of Active Site Mutants of *Escherichia coli* γ-Aminobutyrate Aminotransferase[†]

Wenshe Liu, Peter E. Peterson, James A. Langston, Xueguang Jin, Xianzhi Zhou, Andrew J. Fisher, and Michael D. Toney*

Department of Chemistry, University of California—Davis, Davis, California 95616

Received June 27, 2004; Revised Manuscript Received November 5, 2004

ABSTRACT: The *E. coli* isozyme of γ-aminobutyrate aminotransferase (GABA-AT) is a tetrameric pyridoxal phosphate-dependent enzyme that catalyzes transamination between primary amines and α-keto acids. The roles of the active site residues V241, E211, and I50 in the GABA-AT mechanism have been probed by site-directed mutagenesis. The β-branched side chain of V241 facilitates formation of external aldimine intermediates with primary amine substrates, while E211 provides charge compensation of R398 selectively in the primary amine half-reaction and I50 forms a hydrophobic lid at the top of the substrate binding site. The structures of the I50Q, V241A, and E211S mutants were solved by X-ray crystallography to resolutions of 2.1, 2.5, and 2.52 Å, respectively. The structure of GABA-AT is similar in overall fold and active site structure to that of dialkylglycine decarboxylase, which catalyzes both transamination and decarboxylation half-reactions in its normal catalytic cycle. Therefore, an attempt was made to convert GABA-AT into a decarboxylation-dependent aminotransferase similar to dialkylglycine decarboxylase by systematic mutation of *E. coli* GABA-AT active site residues. Two of the twelve mutants presented, E211S/I50G/C77K and E211S/I50H/V80D, have ∼10-fold higher decarboxylation activities than the wild-type enzyme, and the E211S/I50H/V80D has formally changed the reaction specificity to that of a decarboxylase.

Pyridoxal 5′-phosphate (PLP)[1] is a versatile catalyst in solution, catalyzing a variety of reactions (e.g. transamination, decarboxylation, racemization, etc) with a broad range of amine-containing substrates (*1*). PLP-dependent enzymes catalyze an equally diverse group of reactions and are ubiquitous in biological systems (*2−5*). It has been estimated, for example, that ∼1.5% of the open reading frames in bacterial genomes encode PLP-dependent enzymes (*6*). The protein component of PLP-dependent enzymes endows the coenzyme with much higher catalytic power as well as reaction and substrate specificities. One of the major challenges with PLP-dependent enzymes is understanding how the unique environments of their active sites combine with the basic functionality of the coenzyme to determine reaction specificity.

PLP-dependent enzymes have been grouped based on amino acid sequence homologies (*3−5*). Both GABA-AT and DGD belong to the aminotransferase evolutionary subgroup II (*7*). Multiple sequence alignments of subgroup II enzymes combined with known crystal structures show mechanistically important conservations throughout the sequences, as well as systematic variations in active site

residues that correlate well with known reaction and substrate specificities (*8−12*).

The crystal structure of wild-type GABA-AT and its complex with aminooxyacetate was recently solved using the structure of DGD as a molecular replacement model (*12*). The two structures show strong overall and active site structural similarities, yet they share only 29% sequence identity. Differences in key catalytic residues in the GABA-AT and DGD active sites are expected since GABA-AT catalyzes only transamination (Scheme 2) and DGD catalyzes both decarboxylation and transamination in its normal catalytic cycle (Scheme 3), and the substrate side chain specificity differs between the two enzymes.

Figure 1 presents an overlay of the active sites of *E. coli* GABA-AT and DGD. One sees that the three residues critical to the basic functioning of the coenzyme are identical in both enzymes. In DGD theses are K272, Q246, and D243. K272 forms a Schiff base with PLP, as is found in all PLP-dependent enzymes. Q246 and D243 both interact directly with PLP, hydrogen bonding to the 3′-O and the pyridine N, respectively. The latter residue is thought to maintain the pyridine N in its protonated form, thereby enhancing the electrophilic character of the pyridine ring. R406, which interacts with the substrate α-carboxylate in DGD, is also conserved in GABA-AT (R398) where it is thought to interact with the α-carboxylate groups of α-amino and α-keto acid substrates.

Equally interesting are the differences between DGD and GABA-AT in active site residues. Q52 in DGD is thought to provide a hydrogen bond to the substrate α-carboxylate

* Corresponding author. E-mail: mdtoney@ucdavis.edu. Telephone: 530-754-5282. Fax: 530-752-8995.

[1] Abbreviations: GABA, γ-aminobutyrate; GABA-AT, γ-aminobutyrate aminotransferase; α-KG, α-ketoglutarate; PLP, pyridoxal 5′-phosphate; PMP, pyridoxamine 5′-phosphate; SSDH, succinic semialdehyde dehydrogenase; MDH, malate dehydrogenase; DGD, dialkylglycine decarboxylase; PEPC, phosphoenolpyruvate carboxylase.
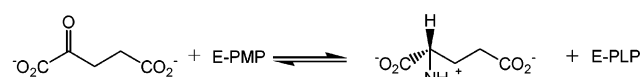
Scheme 1: Stereoelectronic Control of Reactivity in External Aldimine Intermediates
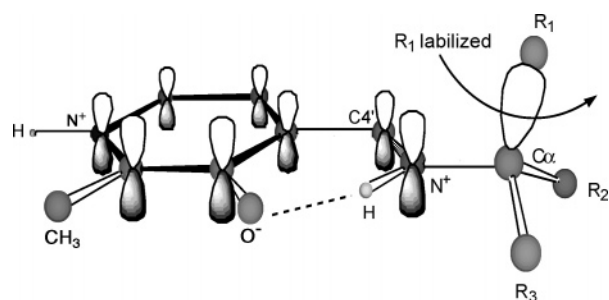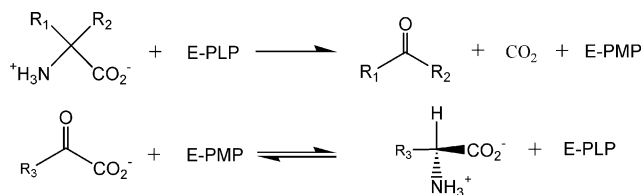

Scheme 2: Reaction Catalyzed by GABA-AT
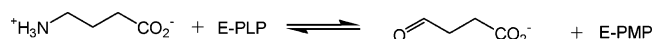
γ-aminobutyrate   succinic semialdehyde

α-ketoglutarate   L-glutamate

Scheme 3: Reaction Catalyzed by DGD

in the decarboxylation half-reaction, thereby activating the carboxylate stereoelectronically by placing the $C\alpha-CO_2^-$ bond parallel to the *p* orbitals of the π bonding system of the external aldimine intermediate (*13*). Scheme 1 illustrates this concept of stereoelectronic control of reactivity in pyridoxal phosphate enzymes, originally put forth by Dunathan (*14*). The structurally equivalent residue in GABA-AT is I50, which is conserved as a hydrophobic residue in all other subgroup II aminotransferases. The specificity of DGD for small 2,2-dialkylglycines (e.g. aminoisobutyrate, isovaline) is thought to originate in the restricted size of the side chain binding pocket formed by W138, M141, and Y301. These residues are changed in GABA-AT to Y138, R141, and G295, respectively, correlating well with the need to bind the distal carboxylate groups of its substrates (*12*). A245 at the back of the PLP ring in DGD is changed to V241 in GABA-AT. We hypothesize that the larger V241 facilitates formation of the obligatory aldimine intermediate between PLP and GABA since this substrate has no α-carboxylate. Finally, S215 in DGD is conserved as E211 in GABA-AT, which is found to interact with either R398 or Y155 (*12*). The structure of the AOA-liganded wild-type enzyme shows E211 neutralizing the charge of R398 in the complex, which may have significant mechanistic implications. Here, the roles of I50, V241, and E211 in GABA-AT in substrate and reaction specificity are determined by analysis of site-directed mutants, and the X-ray structures of the I50Q, V241A, and E211S mutants are presented.

The ease with which the amino acid changes between DGD and GABA-AT can be rationalized based on the

differences in reaction and substrate specificity of the two enzymes suggested that redesign of the GABA-AT active site to contain the decarboxylation apparatus of DGD might be successful at converting GABA-AT into a decarboxylation-dependent aminotransferase specific for dicarboxylate substrates. Such an attempt to alter the reaction specificity of GABA-AT is reported here, with mutations based on information from the structures of GABA-AT and DGD, and multiple sequence alignments of evolutionary subgroup II aminotransferases. A series of twelve site-directed mutants has been constructed and analyzed kinetically. The results show that approximately 10-fold increases in the k_{cat} for decarboxylation are achieved, while approximately 10^6-fold increases in the ratio of decarboxylation to transamination activities of GABA-AT are obtained mainly through reductions in transamination activity.

EXPERIMENTAL SECTION

Materials. GABA, α-KG, carbenicillin, DTT, β-mercaptoethanol, succinic semialdehyde (15% in water), NADPH, PLP, L-glutamate, D-glutamate, D,L-α-methylaspartate, and MDH were purchased from Sigma. D,L-α-methylglutamate was obtained from Acros. Ammonium sulfate, ampicillin, Tris, IPTG, EDTA, ethylene glycol, and lysozyme were from Fisher.

Enzyme Preparations. Wild-type GABA-AT and SSDH were expressed and purified as described previously (*12*). Single mutants (V241A, E211S, and I50Q) were created by site-directed mutagenesis using overlap extension PCR (*15*) and cloned into pET23a. The I50Q/G295Y, E211S/I50G/C77K, and E211S/I50H/V80T mutants were obtained using the Kunkel mutagenesis kit from Bio-Rad and cloned into pET23a. The genes for E211S/I50Q/G295Y/V241A, E211S/I50G, E211S/I50H/V80D, E211S/I50N/V80D, E211S/I50N/V80T, and E211S/I50G/C77R mutants were created by using the Kunkel mutagenesis kit from Bio-Rad and cloned into pET28a, which adds a 6×His tag at the N-terminus of all mutants. Oligonucleotides were from Life Technologies. Full nucleotide sequences of the mutants were determined to confirm the absence of adventitious mutations. The expression and purification of all mutants that did not contain a 6×His tag proceeded as described for wild-type GABA-AT (*12*). The 6×His tag containing mutants were expressed as described for wild-type GABA-AT. The harvested cells were suspended in lysis buffer containing 20 mM potassium phosphate, pH 7.8, 100 μM PLP, 0.5 M KCl, and 0.5 mg/mL lysozyme and stirred on ice for 30 min. The cells were disrupted by sonication, and cell debris was removed by centrifugation for 30 min at 15,000 rpm. The supernatant was mixed with 16 mL Ni^{2+} charged Chelating Sepharose Fast Flow resin from Pharmacia. The mixture was then incubated at room temperature with gentle agitation for 20 min, followed by centrifugation at 500*g* for 4 min. The pellet was carefully decanted and resuspended in 100 mL washing buffer containing 20 mM KH_2PO_4, pH 7.4, 0.5 M KCl, 100 μM PLP, and 10 mM imidazole. It was then centrifuged at 500*g* for 4 min and carefully decanted. The washing step was repeated 3 additional times and another 2 times with increasing imidazole concentrations up to 50 mM. Elution buffer containing 20 mM KH_2PO_4, pH 7.4, 100 μM, 0.5 M KCl, and 250 mM imidazole was then added and mixed together by rotation for 5 min, followed by centrifugation at
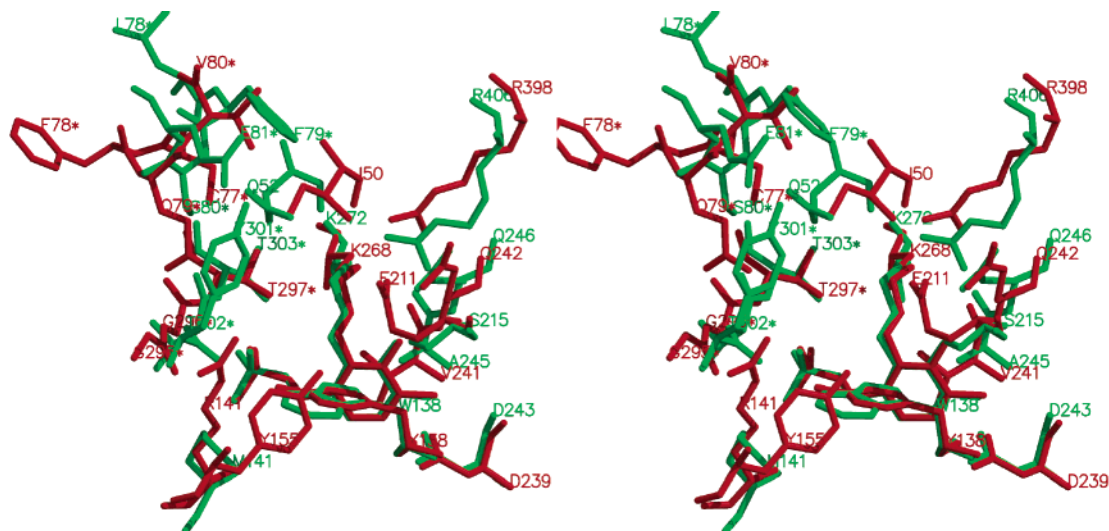
FIGURE 1: Superimposition of the active sites of unbound wild-type *E. coli* GABA-AT (red) and DGD (green). This figure was prepared with Swiss-PdbViewer and MOLSCRIPT.

500g for 4 min. The elution steps were repeated twice more and all the supernatants were collected together and concentrated. The purities of all proteins were analyzed with SDS−PAGE and their concentrations were determined with the Bio-Rad DC assay, using IgG as standard.

GABA Transamination Assay. The reaction was assayed by coupling the succinic semialdehyde produced from the transamination of GABA to the NADP-dependent SSDH reaction, monitoring the increase of NADPH absorbance at 340 nm. The reaction mixtures contained 0.032 μM GABA-AT, 100 mM TEA-HCl, pH 7.8, 5 mM DTT, 1 mM EDTA, 100 μM PLP, 100 mM KCl, 500 μM NADP, 3 units SSDH, and six concentrations of GABA at six different fixed concentrations of α-KG. All assay components were initially mixed together except for *E. coli* GABA-AT, and incubated for 5 min at 25 °C. The reactions were initiated by adding GABA-AT in a small volume.

For the V241A, E211S, I50Q, I50Q/G295Y, E211S/I50G/C77K, and E211S/I50H/V80T mutants, GABA transamination assays were performed as described for wild-type GABA-AT, except that different concentrations of enzyme and substrates were used to obtain easily measurable absorbance changes. Since the activities of the other mutants are relatively low, assays were performed with 100 mM GABA and 10 mM α-KG.

Nonlinear regression for systems containing two or more independent variables was performed with GraFit 4.05, while data sets containing a single independent variable were fitted using Kaleidagraph 3.6.

Inhibition Assay. The SSDH coupled assay described above was employed for inhibition assays with wild-type GABA-AT, V241A, and I50Q. Initial rates of GABA transamination in the presence of six concentrations of the inhibitors (succinate, maleate, glutarate, and aminooxyacetate) were measured. The inhibition mechanisms for all inhibitors were assumed to be competitive on the basis of the structural similarities between the substrates of GABA-AT and the inhibitors. The reaction mixtures contained 100 mM TEA-HCl, pH 7.8, 5 mM DTT, 1 mM EDTA, 100 μM PLP, 100 mM KCl, 500 μM NADP, 3 units SSDH, GABA-AT, GABA, α-KG, and varying concentrations of the inhibitors. The concentrations of GABA and α-KG are 10

mM and 2 mM for wild-type GABA-AT, 100 mM and 50 mM for I50Q, and 10 mM and 2 mM for V241A, respectively.

L-Aspartate Aminotransferase Activity Assay. The oxaloacetate produced from L-aspartate transamination of wild-type GABA-AT was coupled to the MDH reaction and the decrease of NADH absorbance at 340 nm was monitored (*16*). The reaction mixtures contained 9.2 μM GABA-AT, 100 mM TEA-HCl, pH 7.8, 5 mM DTT, 1 mM EDTA, 100 μM PLP, 100 mM KCl, 250 μM NADH, and 10 units MDH, six concentrations of L-aspartate at 5 mM α-KG or six concentrations of α-KG at 100 mM L-aspartate. All assay components were initially mixed except for GABA-AT and incubated for 5 min at 25 °C. The reactions were initiated by adding GABA-AT in a small volume. The L-aspartate aminotransferase activity of E211S was analyzed similarly, except that 0.02 mM α-KG was used with varying L-aspartate concentrations.

Decarboxylation Assays. Four amino acids (L-glutamate, D-glutamate, D,L-α-methylglutamate, and D,L-α-methylaspartate) were tested for wild-type GABA-AT and all mutants made. CO_2 produced from the decarboxylation of these substrates was assayed with a carbon dioxide detection kit from Sigma Diagnostics. The method is based on conversion of phosphoenolpyruvate and CO_2 into oxaloacetate by PEPC, followed by the subsequent MDH catalyzed reduction of oxaloacetate by NADH to produce malate and NAD. The decrease in NADH absorbance at 340 nm was followed. The reaction conditions were: 80 mM amino acid substrate (L-glutamate, D-glutamate, D,L-α-methylglutamate, D,L-α-methylaspartate), 2.4 mM α-ketoglutarate, 40 μM PLP, 366 μM NADH, 800 μL Reagent A of the CO_2 detection kit (containing 2.2 mM phosphoenolpyruvate, 0.32 mM NADH, 10 mM Mg^{2+}, buffer, pH 8.0, and 0.05% sodium azide), and 80 μL Reagent B of the CO_2 detection kit (containing 2.75 units/mL PEPC, 15.4 units/mL MDH, 10 mM Mg^{2+}, and buffer, pH 6.5) in 1 mL total reaction solutions. The enzyme concentrations were varied to obtain easily measurable absorbance changes. The deionized H_2O used to prepare all reagents was purged with Argon bubbled through two 10 M KOH scrubbers to remove CO_2. A blank was assayed along with each amino acid substrate, in which GABA-AT (or

mutant) was replaced by CO_2-free deionized H_2O. The activity of the blank was subtracted from the activity of the sample. Assays were performed by first combining all ingredients except Reagent B and GABA-AT (or mutant) and incubating 5 min at 25 °C. Next, Reagent B was added and followed by another 10 min incubation to remove any background caused by dissolved CO_2. Then GABA-AT (or mutant) was added and the reactions were followed for 70 min. Typically, the first 5 min showed a small burst of absorbance change due to dissolved CO_2 in the enzyme solution. Therefore, this initial data was discarded. Additionally, $NaHCO_3$ was added to 800 μM after each assay to confirm that the coupling enzymes were active. This CO_2 assay was tested with AIB decarboxylation of DGD. Kinetic parameters for decarboxylation of AIB by DGD obtained with this assay were within error of those obtained using a secondary alcohol dehydrogenase coupled assay (*17*).

Crystallization, X-ray Diffraction Data Collection, and Structure Determination of I50Q, V241A, and E211S. Crystals of I50Q, V241A, and E211S were obtained by the hanging drop vapor diffusion method using a slight modification of the protocol described in a previous publication (*12*). One microliter of enzyme at approximately 25 mg/mL in 70 mM potassium phosphate, pH 7.6, 100 μM PLP, and 1 mM DTT was mixed with an equal volume of reservoir solution containing 0.1 M HEPES–KOH, pH 7.6, 100 μM PLP, and 1.2–1.6 M $(NH_4)_2SO_4$ and equilibrated against 1 mL of this reservoir solution. Crystals generally appeared in a week and reached their maximal dimensions after three weeks. Crystals for data collection were cryoprotected using 30% ethylene glycol in the mother liquor for 2 h. They were mounted in a loop and flash frozen in a nitrogen steam at 100 K. Data were collected for I50Q on a Proteum 6000 CCD using Cu Kα radiation, for V241A on a Mar 345 image plate using the synchrotron beamline 9–1 at Stanford Synchrotron Radiation Laboratory at a wavelength of 0.98 Å, and for E211S on an RAXIS IV image plate using Cu Kα radiation. Reflection intensities were integrated with DENZO, and merged and reduced to structure factors using the SCALEPACK, CAD, and TRUNCATE programs from the CCP4 suite (*18*). Since the space group and unit cell parameters are identical to those of the wild-type enzyme (pdb code 1SF2), the structures of all three mutants were determined using the wild-type structure as an initial model for simulated annealing using CNS after PLP, ethylene glycol, sulfate ions, and water molecules had been removed. The models were further refined with energy minimization and B-factor refinement combined with manual adjustments using the program O. F_o-F_c and $2F_o-F_c$ electron density maps as well as omit maps were calculated at regular intervals to allow fitting and modification. Omit maps for the active sites of I50Q and V241A clearly indicated that there are two cofactor forms (PLP and PMP) bound with partial occupancies at the same site, with alternative conformations of K268. Only PMP is found in the active site of E211S. Both PLP and PMP were generated, assigned occupancies of 50%, and refined as alternative ligands for I50Q and V241A.

Since there is no facility in CNS for multiple ligand generation, this was done manually. The coordinates of both ligands were read as structure input files of generate.inp of CNS to output molecular topology files and coordinate files

Table 1: Data Collection and Refinement Statistics

	I50Q	V241A	E211S
unit cell dimensions			
$a = b$,	108.12,	108.20,	108.26,
c (Å)	301.75	301.66	300.83
space group	$P3_221$	$P3_221$	$P3_221$
resolution range (Å)	30.0–2.1	30.0–2.5	30.0–2.52
$R_{sym}{}^a$ (%)	7.1	3.9	8.4
$\langle I\rangle/\sigma\langle I\rangle$	9.4	27.1	12.4
no. of reflections	115 075	68 806	69 918
redundancy	3.5	12.3	5.5
completeness (%)	95.8	98.1	97.5
$R_{factor}{}^b$ (%)	16.9	15.4	18.7
$R_{free}{}^c$ (%)	20.6	20.2	24.0
cofactors and occupancy	PLP (0.5), PMP (0.5)	PLP (0.5), PMP (0.5)	PMP
no. of protein atoms	12 828	12 816	12 812
no. of cofactor atoms	60^d or 64^e	60^d or 64^e	64
no. of water molecules	1122^d or 1121^e	955^d or 951^e	673
no. of sulfate atoms	75	55	80
no. of ethylene glycol atoms	68	56	52
mean B-factor (Å^2)			
entire molecule	24.82	26.98	38.79
main chain	22.85	25.24	37.52
side chains	25.31	27.25	39.64
solvent	31.9	32.75	36.45
rmsd from ideality			
bond distances (Å)	0.011	0.010	0.007
bond angle (deg)	1.53	1.44	1.31

^{a} $R_{sym} = \sum\sum_j|I_j(hkl) - \langle I(hkl)\rangle|/\sum\sum_j|I(hkl)|$, where I_j is the measured intensity of reflection j and $\langle I\rangle$ is the mean intensity over j reflections. ^{b} $R_{factor} = \sum||F_o(hkl)| - |F_c(hkl)||/\sum|F_o(hkl)|$, where F_o and F_c are observed and calculated structure factors, respectively. No σ-cutoff was applied. ^{c} R_{free} is calculated with 5% of the data that were not used for refinement. ^{d} Enzyme structures with PLP bound. ^{e} Enzyme structures with PMP bound.

containing both. Then, both the coordinate files and the topology files were manually modified to insert the SEGID AC1-DC1 for the four PLP cofactors and SEGID AC2-DC2 for the four PMP cofactors. In the subsequent refinement, the interactions between AC1-DC1 and AC2-DC2 were omitted. It was also found that there are alternative confirmations for residues 112 and 217 in all four chains of I50Q, and for residue 112 in chains A and D of E211S. The alternative conformations of those residues as well as K268 were generated and refined as described in the previous publication (*12*). The aldimine adduct formed between K268 and PLP in I50Q and V241A was added as a protein patch during refinements. The final refinement statistics are listed in Table 1. The coordinates have been deposited in the Protein Data Bank (PDB codes: I50Q, 1SZS; V241A, 1SZU; E211S, 1SZK).

RESULTS

Wild-Type GABA Transamination Activity. GABA-AT catalysis follows a ping-pong mechanism. The initial velocities measured at six concentrations of α-KG with six different concentrations of GABA are presented in Figure 2A. The data suggest that substrate inhibition occurs with α-KG but not with GABA. This is confirmed by double reciprocal plots for both GABA (Figure 2B) and α-KG (Figure 2C). The double reciprocal plot for GABA shows parallel lines at low α-KG concentrations, indicating no substrate inhibition. However, the plot for α-KG shows nonlinear curves indicating competitive substrate inhibition by α-KG against GABA, due to α-KG binding to the PLP form of GABA-AT. The entire data set was fitted by nonlinear regression to eq 1 (*19*).

$$V_i =$$

$$\frac{V_{max}[GABA][KG]}{K_{GABA}[KG]\left(1 + \dfrac{[KG]}{K_i^{KG}}\right) + K_{KG}[GABA] + [GABA][KG]} \quad (1)$$

Here, V_i is the initial velocity, V_{max} the maximal velocity, K_{GABA} the Michaelis constant for GABA, K_{KG} the Michaelis constant for α-KG, and K_i^{KG} the competitive inhibition constant for α-KG binding to the PLP form of GABA-AT. The results from the fitting are given in Table 2.

Mutant GABA Transamination Activity. The measurement of the mutant activities was carried out as for wild-type GABA-AT. For mutants with $k_{cat} \leq 0.01$ s^{-1}, kinetic analysis was performed only at 100 mM GABA and 5 mM α-KG. For mutants with higher activities, full kinetic analyses were undertaken. Initial velocities were measured for five GABA concentrations at each of five fixed concentrations of α-KG. The data were fitted to eq 2, except for the I50Q mutant. The kinetic parameters obtained from the analyses are presented in Table 2.

$$V = \frac{V_{max}[GABA][KG]}{K_{GABA}[KG] + K_{KG}[GABA] + [GABA][KG]} \quad (2)$$

The data for I50Q show substrate inhibition for both GABA and α-KG. The nonlinearity of double reciprocal plots for GABA and α-KG (data not shown) confirms this. The data were fitted to eq 3.

$$V = V_{max}[GABA][KG] \Bigg/ \left\{ K_{GABA}[KG]\left(1 + \frac{[KG]}{K_i^{KG}}\right) + \right.$$
$$\left. K_{KG}[GABA]\left(1 + \frac{[GABA]}{K_i^{GABA}}\right) + [GABA][KG] \right\} \quad (3)$$

Here K_i^{GABA} is the inhibition constant for GABA binding to the PMP form of GABA-AT. The parameters obtained are presented in Table 2.

L-Asparate Aminotransferase Activity of Wild-Type GABA-AT and E211S. The L-aspartate aminotransferase activity of both wild-type GABA-AT and E211S was determined by varying the L-aspartate concentration at 5 mM α-KG, and varying α-KG concentration at 100 mM L-aspartate. The data for wild-type GABA-AT were fitted to eq 4, where S is either L-aspartate or α-KG.

$$V_i = \frac{V_{max}[S]}{K_S + [S]} \quad (4)$$

The parameters obtained for wild-type GABA-AT are $k_{cat}^{app} = 0.016 \pm 0.003$ s^{-1}, $K_{L-asp}^{app} = 150 \pm 50$ mM, and $K_{KG}^{app} = 0.8 \pm 0.4$ mM. The data for E211S show substrate inhibition by α-KG. The data at varying concentrations of L-asparate were fitted to eq 4, while the data for varying α-KG were fitted to eq 5.

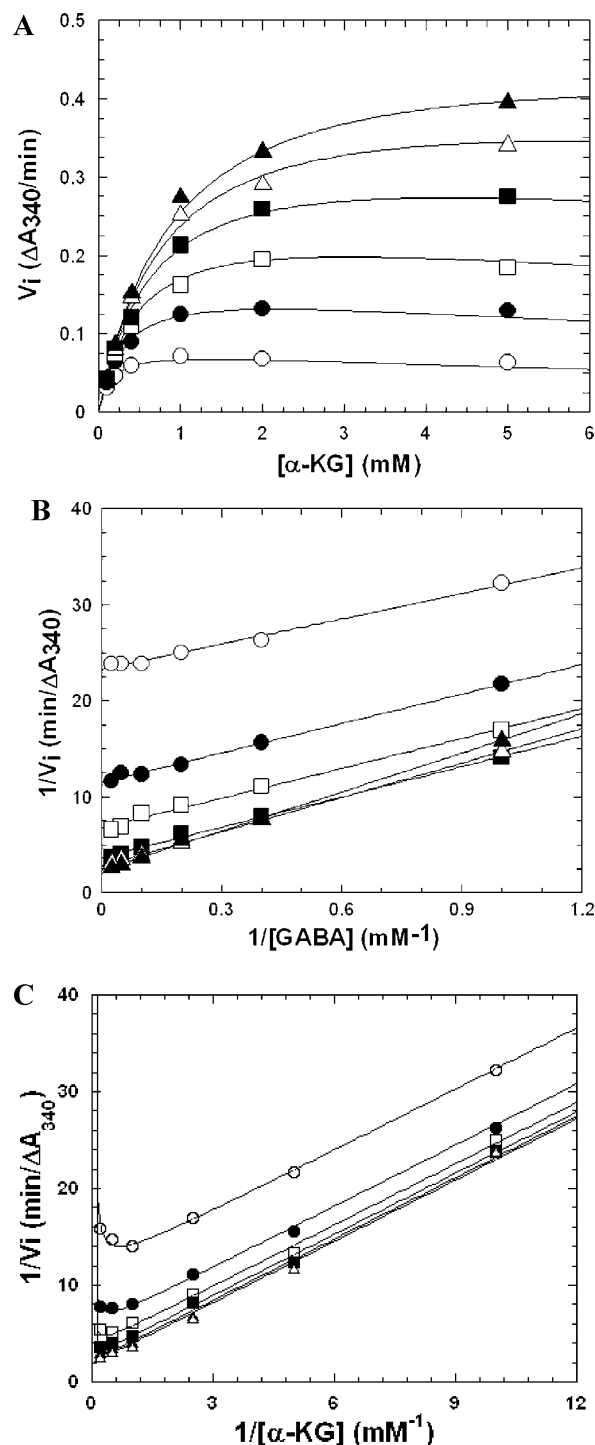$$V_i = \frac{V_{max}[KG]}{K_{KG} + \dfrac{[KG]^2}{K_i^{KG}} + [KG]} \quad (5)$$

FIGURE 2: (A) Plot of wild-type GABA-AT transamination initial velocity vs α-KG concentration. GABA concentrations: 1 mM (○), 2.5 mM (●), 5 mM (□), 10 mM (■), 20 mM (△), and 40 mM (▲). The solid curves are from the global nonlinear regression fit to eq 1. (B) Double reciprocal plot of initial velocity vs GABA concentration. α-KG concentrations: 0.1 mM (○), 0.2 mM (●), 0.4 mM (□), 1 mM (■), 2 mM (△), and 5 mM (▲). The solid curves are linear fits to the data. (C) Double reciprocal plot of initial velocity vs α-KG concentration. GABA concentrations: 1 mM (○), 2.5 mM (●), 5 mM (□), 10 mM (■), 20 mM (△), and 40 mM (▲).

Here, K_i^{KG} is the α-KG inhibition constant. The parameters obtained for E211S are $k_{cat}^{app} = 0.073 \pm 0.005$ s^{-1}, $K_{L-asp}^{app} = 56 \pm 8$ mM, $K_{KG}^{app} = 0.0018 \pm 0.0003$ mM, and $K_i^{KG} = 0.20 \pm 0.06$ mM. The K_{KG}^{app} values for wild-type GABA-AT and E211S determined here in the L-aspartate aminotransferase assay are close to the values of K_{KG} obtained

Table 2: GABA/α-Ketoglutarate Transamination Analysis of Wild-Type GABA-AT and Its Mutants[a]

	k_{cat} (s^{-1})	k_{cat}/K_{GABA} (M^{-1} s^{-1})	K_{GABA} (mM)	K_{KG} (mM)	K_i^{KG} (mM)
wild type	47.4	8172	5.8	1.07	10.2
	(1.0)	(590)	(0.4)	(0.05)	(2.3)
V241A	1.93	64	30	0.13	
	(0.08)	(6)	(2)	(0.01)	
E211S	0.56	6.5	86	0.0021	0.20[d]
	(0.06)	(0.9)	(9)	(0.0004)	(0.06)
I50Q[e]	13.5	199	68	46	178
	(0.3)	(18)	(6)	(3)	(31)
I50Q/G295Y	0.028	5.9	4.7	0.78	
	(0.001)	(0.3)	(0.2)	(0.04)	
E211S/I50Q/ G295Y/V241A[b]	0.004 (0.001)				
E211S/I50G[b,c]	0.003 (0.001)				
E211S/I50G/ C77K	0.25 (0.01)	42 (2)	5.9 (0.2)	0.72 (0.03)	
E211S/I50G/ C77R[b,c]	0.0005 (0.0003)				
E211S/I50H/ V80T	0.106 (0.004)	0.73 (0.09)	146 (18)	0.063 (0.006)	
E211S/I50H/ V80D[b,c]	0.00023 (0.00010)				
E211S/I50N/ V80T[b,c]	0.0058 (0.0021)				
E211S/I50N/ V80D[b,c]	0.0075 (0.0027)				

[a] Standard errors from nonlinear regression are given in parentheses. Conditions: 25.0 °C, 100 mM TEA-HCl, pH 7.8, 100 mM KCl, 5 mM DTT, 1 mM EDTA, 100 μM PLP, 500 μM NADP, and 3 units SSADH. [b] Based on the limit of detection of the assay, assuming saturation of the enzyme by substrates. [c] These mutants have a 6-His tag at the N-termini. [d] The value was obtained from the L-aspartate transamination assay. [e] K_i^{GABA} = 670(145) mM.

from GABA transamination assays. α-KG shows substrate inhibition with E211S. This was not found in the GABA transamination assay where the concentrations of α-KG used were not high enough for it to be observed. Thus, α-KG substrate inhibition is observed with wild-type GABA-AT, I50Q, and E211S, and might also be observed with the other mutants if the α-KG concentrations were increased sufficiently.

Inhibition Studies. Succinate, maleate, glutarate, and aminooxyacetate were assumed to be competitive inhibitors against transamination since their structures are similar to GABA. The inhibition data measured were fitted to eq 6.

$$V = \frac{V_{max}[\text{GABA}][\text{KG}]}{K_{GABA}[\text{KG}]\left(1 + \frac{[\text{I}]}{K_i}\right) + K_{KG}[\text{GABA}] + [\text{GABA}][\text{KG}]}$$

(6)

Here, K_i is the inhibition constant for binding to the PLP form of GABA-AT, K_{GABA} is the Michaelis constant for GABA, and K_{KG} is the Michaelis constant for α-KG. Since the concentration of α-KG used for wild-type GABA-AT and the concentrations of GABA and α-KG used for I50Q are much lower than the values of their competitive inhibition constants, the substrate inhibitions in the inhibition assays of both enzymes were negligible. For V241A, substrate inhibition was not detected. The values of K_{GABA} and K_{KG}

Table 3: Competitive Inhibition Constants[a]

	succinate (mM)	maleate (mM)	glutarate (mM)	aminooxyacetate (μM)
wild type	27	3.9	19	0.62
	(1)	(0.1)	(3)	(0.12)
V241A	720	780	140	1.13
	(50)	(60)	(10)	(0.01)
I50Q	197	46	233	0.24
	(13)	(1)	(6)	(0.03)

[a] Standard errors from nonlinear regression are given in parentheses. Conditions: 25 °C, 100 mM TEA-HCl, pH 7.8, 100 mM KCl, 5 mM DTT, 1 mM EDTA, 100 μM PLP, 500 μM NADP, and 3 units/mL SSDH. The concentrations of GABA and α-KG were 10 and 2 mM, respectively, for wild-type GABA-AT, 10 and 2 mM for V241A, and 100 and 50 mM for I50Q.

for wild-type GABA-AT, I50Q, and V241A in Table 2 were employed in eq 6. Least-squares fitting of the inhibition data to eq 6 gave the K_i values of the above four inhibitors, which are presented in Table 3.

Decarboxylation Activity. Four amino acids (L-glutamate, D-glutamate, D,L-α-methylglutamate, D,L-α-methylaspartate) were tested as substrates for decarboxylation assays. The values of k_{cat} for wild type and mutants are presented in Table 4. Wild-type GABA-AT has low activity as a decarboxylase (k_{cat} for transamination is ∼8 × 10^5-fold greater than k_{cat} for decarboxylation). V241A and I50Q/G295Y do not show detectable activity with any amino acid tested. Neither I50Q nor E211S show dramatic improvements in decarboxylation activity over wild type. Since the structurally homologous position in DGD corresponding to E211 in GABA-AT is a conserved serine, the E211S mutant was selected as a template for further mutagenesis studies.

The k_{cat} values for the additional E211S-based mutants are presented in Table 4. None gives a dramatic increase in decarboxylation activity with any of the four substrates tested. However, the mutant E211S/I50H/V80D does show significant increases: 10-fold with L-glutamate, 6.4-fold with D-glutamate, and 2-fold with D,L-α-methylglutamate. The E211S/I50G/C77K also gives a 9-fold increase in activity with L-glutamate. The lower activity of all the mutants with D,L-α-methylaspartate may be due to the weaker binding of D,L-α-methylaspartate caused by the E211S mutation (Liu and Toney, unpublished results). Table 4 also presents the ratio of k_{cat} for decarboxylation with different substrates to that of GABA transamination for each enzyme. Large increases in this ratio are observed with the E211S/I50H/ V80D and E211S/I50G/C77R mutants, mainly due to greatly decreased transamination activities.

Crystal Structures of I50Q, V241A, and E211S. All three structures were solved by molecular dynamics refinement using wild-type GABA-AT as the initial model. The overall structures for all three mutants show no significant differences with wild-type GABA-AT. Overlays of the Cα traces of the tetramers of I50Q, V241A, and E211S with wild-type GABA-AT result in rms deviations of 0.34, 0.25, and 0.27 Å, respectively.

Figure 3A presents the electron density map for the active site of I50Q. The map indicates two cofactor forms (PLP and PMP with partial occupancies) and the original I50 residue is clearly a glutamine. The active site structure of I50Q is very similar to that of wild-type GABA-AT except for the mutation, the orientations of Q79* and E211, and

Table 4: Decarboxylation Analysis of Wild-Type GABA-AT and Its Mutants[a]

	L-glutamate		D-glutamate		D,L-α-methyl glutamate		D,L-α-methyl aspartate	
	k_{cat} $(\times 10^4\ s^{-1})$	ratio $(\times 10^4)$	k_{cat} $(\times 10^4\ s^{-1})$	ratio $(\times 10^4)$	k_{cat} $(\times 10^4\ s^{-1})$	ratio $(\times 10^4)$	k_{cat} $(\times 10^4\ s^{-1})$	ratio $(\times 10^4)$
wild type	0.6 (0.2)	0.012 (0.004)	1.5 (0.3)	0.032 (0.007)	9.2 (0.9)	0.19 (0.02)	8.6 (0.2)	0.18 (0.01)
V241A	ND		ND		ND		ND	
E211S	1.6 (0.9)	2.9 (1.6)	1.8 (0.2)	3.2 (0.5)	2.4 (0.6)	4.3 (1.1)	ND	
I50Q	2.2 (0.2)	0.16 (0.02)	1.0 (0.3)	0.074 (0.023)	7.0 (0.2)	0.52 (0.02)	4.0 (0.2)	0.30 (0.02)
I50Q/G295Y	ND		ND		ND		ND	
E211S/I50Q/ G295Y/V241A	ND		ND		ND		ND	
E211S/I50G[b]	0.9 (0.3)	300 (140)	ND		1.1 (0.4)	370 (180)	ND	
E211S/I50G/ C77K[b]	5.2 (0.7)	21 (3)	6.9 (1.0)	28 (4)	10.4 (1.0)	42 (4)	3.8 (0.7)	15 (3)
E211S/I50G/ C77R[b]	1.9 (0.6)	3800 (2300)	1.1 (0.8)	2200 (2100)	ND		1.4 (0.5)	2800 (1700)
E211S/I50H/ V80T[b]	ND		1.5 (0.3)	14 (3)	ND		1.4 (0.1)	13 (1)
E211S/I50H/ V80D[b]	6.1 (0.9)	2.7×10^4 (1.2)	9.8 (1.4)	4.3×10^4 (1.9)	17 (3)	7.4×10^4 (3.2)	7.4 (0.4)	3.2×10^4 (1.4)
E211S/I50N/ V80T[b]	1.9 (0.3)	330 (120)	ND		2.8 (0.5)	480 (190)	1.4 (0.3)	240 (90)
E211S/I50N/ V80D[b]	ND		ND		ND		ND	

[a] Standard errors from nonlinear regression are given in parentheses. CO_2 detection is based on the conversion of phosphoenolpyruvate and CO_2 into oxaloacetate by PEPC, followed by MDH catalyzed conversion of oxaloacetate and NADH to malate and NAD^+. No activity is detected (ND) when k_{cat} is smaller than $2 \times 10^{-5}\ s^{-1}$. The "ratio" column for each amino acid substrate is the ratio of k_{cat} for decarboxylation of the amino acid to k_{cat} for GABA transamination by the given enzyme. [b] These mutants have a 6-His tag at their N-termini.

the presence of two cofactor forms. The Q79* side chain twists toward G296*. The new Q79* side chain orientation is stabilized by three hydrogen bonds involving the amide side chain, formed with a water molecule, a sulfate ion, and the backbone oxygen of G296*. E211 in I50Q takes on a different orientation compared to that in wild-type GABA-AT; the side chain rotates around the Cβ–Cγ bond by ~180°. The site where the E211 carboxylate group is found in wild-type GABA-AT is filled by an ethylene glycol molecule in I50Q. The new orientation of E211 is stabilized by three hydrogen bonds to the side chain carboxylate group: two with water molecules and one with Y155. In the PLP form, K268 and PLP form an aldimine bond as in wild-type GABA-AT. However, in the PMP form, K268 takes on a new orientation, hydrogen bonding to T297*, and the amino group of PMP rotates toward E211. The side chain amide of Q50 is involved in an average (over the four monomers in the asymmetric unit) of two hydrogen bonds, one to the sulfate ion and another to a water molecule. The amide oxygen forms a hydrogen bond with K268 in the PMP form.

Figure 3B presents the electron density at the active site of V241A. The cofactor exists in both PLP and PMP forms. A water molecule fills the void left by the mutation from V241 to alanine. When the cofactor is in the PMP form, the K268 amino group moves toward T297* forming a hydrogen bond. The PMP amino group rotates toward E211.

The electron density map of the active site of E211S is shown in Figure 3C. Only one cofactor form (PMP) is indicated by the density. Extra density in the active site has been assigned as a sulfate ion, which is reasonable since the mutation removes a negative charge from the active site. K268 takes on a similar orientation to that in the PMP form of V241A, forming a hydrogen bond with T297*. The PMP amino group flips toward Y138 and makes a strong salt bridge with the sulfate ion. The Cβ–Oγ bond in the introduced S211 residue has the same orientation as the Cβ–Cγ bond in I50Q. The S211 hydroxyl group makes a hydrogen bond with a water molecule.

An overlay of wild-type GABA-AT and the I50Q, V241A, and E211S mutants is shown in Figure 3D. The structures are all remarkably similar except for the sites of the mutations, as noted above.

DISCUSSION

GABA-AT from *E. coli* is a typical PLP-dependent evolutionary subgroup II aminotransferase that acts on both primary amine and α-amino acid substrates (*3, 4*). The overall GABA-AT catalyzed reaction consists of two half-reactions, in which the cofactor alternates between its aldehydic (PLP) and amino (PMP) forms (Scheme 2). GABA is converted to succinic semialdehyde in the first half-reaction, and α-KG is converted to L-glutamate in the second. The ping-pong mechanism is evidenced by the parallel double reciprocal lines at lower concentrations of α-KG in Figure 2B. The larger slopes at higher concentrations of α-KG in Figure 2B and the upwardly curving data in Figure 2C are due to inhibition of the PLP enzyme by α-KG, which is competitive with respect to GABA. Similar inhibition by α-KG has been observed with aspartate aminotransferase (*20−23*).

DGD is a PLP-dependent enzyme that is also a member of the aminotransferase evolutionary subgroup II (*7, 8*). It is unusual for this group of enzymes in that it does not catalyze two simple transamination half-reactions but rather
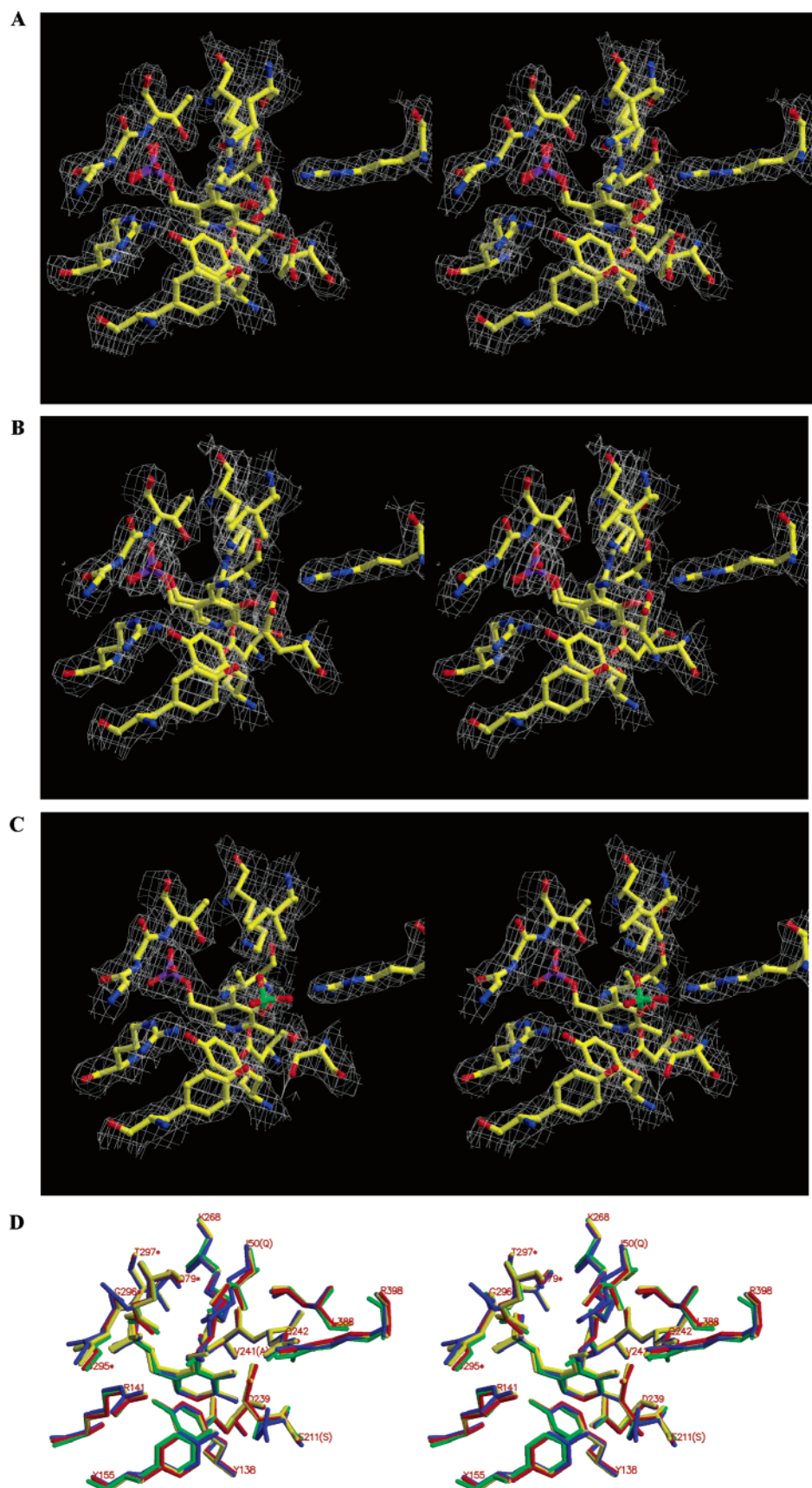
FIGURE 3: (A) $2F_o-F_c$ electron density map for the active site region of I50Q. The map is contoured at 1.2σ. Both PLP and PMP, and alternative conformations of K268, are observed. (B) $2F_o-F_c$ electron density map for the active region of V241A. The map is contoured at 1.2σ. Both PLP and PMP, and alternative conformations of K268, are observed. (C) $2F_o-F_c$ electron density map for the active site region of E211S. The map is contoured at 1.2σ. The cofactor is found only as PMP in this structure. (D) Superimposition of the active site structures of wild-type GABA-AT (in red), I50Q (in blue), V241A (in yellow), and E211S (in green). Parts A, B, and C were prepared with BOBSCRIPT (27, 28). Part D was prepared with MOLSCRIPT(27, 28).

an oxidative decarboxylation of 2,2-dialkylglycines with concomitant amino group transfer to the coenzyme in its first half-reaction, followed by amino group transfer from the coenzyme to an α-keto acid (e.g. pyruvate) in its second (Scheme 3). The structure of DGD was used as a molecular replacement model in the original solution of the *E. coli* GABA-AT structure, and the refined models show strong similarities both in overall fold and active site structure (*12*).

The roles of the active site residues V241, E211, and I50 in the GABA-AT mechanism have been probed here by site-directed mutagenesis. The first GABA-AT mutant presented in Table 2 is V241A, which changes the β-branched valine residue located immediately behind the pyridine ring (Figure 3D). DGD is unique among subgroup II aminotransferases in having an alanine at this position; all others members of this group have either valine or isoleucine. Since DGD is unique in this group in utilizing α-amino acids in both half-reactions, we hypothesized that the β-branched side chain in the other enzymes is required to destabilize sterically the internal aldimine formed between the active site lysine and PLP so that the primary amine substrates could more easily displace this lysine in the transimination reaction required to form the obligatory substrate-PLP Schiff base (external aldimine) intermediate. That is, in DGD the interaction between R406 and the substrate α-carboxylate facilitates external aldimine formation whereas in the primary amine half-reactions of the other subgroup II enzymes the β-branched side chain behind PLP is required to promote external aldimine formation by sterically destabilizing the internal aldimine. The V241A mutant is therefore predicted to have a higher K_{GABA} than wild-type enzyme since the internal aldimine form of the enzyme should be selectively stabilized by the mutation. This prediction is borne out by the results presented in Tables 2 and 3, which show a 5-fold higher K_{GABA} and a 2-fold higher K_i^{AOA}. The inhibition results with the noncovalently binding dicarboxylate inhibitors presented in Table 3 (i.e. succinate, maleate, and glutarate) suggest that the Michaelis complex for dicarboxylate substrates has been significantly destabilized by the mutation. The ~6-fold reduced K_{KG} value additionally suggests a destabilization of the unliganded PMP form of the enzyme by the mutation.

The mechanistic role of E211 in GABA-AT is thought to be to neutralize the positive charge of R398 in the primary amine half-reaction where the substrate does not contain an α-carboxylate group. In the α-KG/L-glutamate half-reaction the substrate carboxylate fulfills this charge-neutralization role, with E211 rotating out of the substrate binding site to interact with Y155 as seen in the structure of the I50Q mutant. The E211S mutant probes the role of E211 in GABA-AT and is predicted by the above reasoning to have a lower k_{cat} value due to the deleterious effects of the leaving R398 unneutralized on the reaction energetics of the primary amine half-reaction, to have a higher K_{GABA} for a similar reason, and to have a lower K_{KG} since the α-KG carboxylate no longer must compete with the E211 side chain carboxylate for interaction with R398. These predictions are again borne out by the results presented in Table 2. The k_{cat} value is lower by ~100-fold while K_{GABA} is ~15-fold higher and K_{KG} is 500-fold lower. These results and the observation of E211 in the two alternative conformations in the X-ray structures provides conclusive evidence for the role of this amino acid in charge-neutralizing R398 in the primary amine half-

reaction. Additional evidence in support of this conclusion is provided by the results of aspartate aminotranferase activity measurements, which employ only α-amino and α-keto acid substrates (L-asparate and α-KG) and not primary amines. The k_{cat} value for E211S is ~5-fold higher than that for wild type, while the K_{L-asp} and K_{KG} values are 3-fold and 440-fold lower. The larger decrease for K_{KG} vs K_{L-asp} probably originates from greater stabilization of the amino group of PMP by E211, via electrostatic interactions, compared to the PLP Schiff base with K268. The E211S mutation would selectively destabilize the PMP enzyme, causing a selective lowering of K_{KG}.

The I50Q mutant was made for a 2-fold purpose, to test the importance of the conserved I50 located at the "top" of the GABA-AT active site (Figure 1) and to introduce the DGD active site residue thought to be most important to the facilitation of α-amino acid decarboxylation (*13*). The most remarkable quality of this mutant is the 12-fold higher K_{GABA}, the 43-fold higher K_{KG}, and the ~10-fold higher K_i values for the noncovalently binding inhibitors reported in Table 3. These higher values are most readily interpreted in terms of the longer Q50 side chain sterically inhibiting access of the substrates and inhibitors to the binding site (Figures 3A and 3D). The role of I50 in the wild-type enzyme is apparently that of a lid that restricts the size of the substrate binding pocket.

The decarboxylation activity of I50Q was measured, as were those of the other mutants and the wild-type enzyme (Table 4). The mutation has a negligible effect, in reference to wild type, on the enzyme's ability to catalyze decarboxylation of the four amino acids tested. This result is readily understood from the X-ray structure; the location of the Cα atoms of Q52 in DGD and I50 in GABA-AT are 2.3 Å apart, with that of I50 being closer to the substrate binding site (Figure 1). Additionally, in DGD the backbone amide N of S80 and the phenolic hydroxyl of Y301 hydrogen bond to the amide oxygen of Q52, holding it in the proper orientation to interact with the substrate carboxylate. Similar orienting interactions in GABA-AT are not present to position the side chain amide of the I50Q mutant.

As mentioned above, the active site residue Y301 in DGD hydrogen bonds to the Q52 amide oxygen, helping to keep it positioned to bind to the substrate α-carboxylate. The corresponding residue in GABA-AT was mutated to give the G295Y mutant in the context of the I50Q mutant. The G295Y mutation further reduces the I50Q k_{cat} by ~400-fold but causes the K_{GABA} and K_{KG} values to be reduced to wild-type values. The results of decarboxylation assays reported in Table 4 show that the addition of the G295Y mutation to the I50Q mutation only lowers the enzyme's ability to catalyze decarboxylation, suggesting that the desired orienting interactions between the tyrosine and glutamine side chains is not obtained. Figure 1 shows that Q79 in GABA-AT is located in front of G295 and the introduced tyrosine at this position may well incur steric clashes with the Q79 side chain.

The E211S/I50Q/G295Y/V241A quadruple mutant incorporates all of the primary differences in active site structure thought to engender decarboxylase activity in DGD. Based on the results with the component mutations, it is not unexpected that this mutant shows only very low transamination activity and undetectable decarboxylase activity,

further emphasizing the intricacies of protein structural interactions required to give altered reaction specificity.

The results discussed above strongly suggested that the side chain introduced by the I50Q mutation was not facilitating substrate carboxylate binding in the stereoelectronically activated position, rather hindering it sterically. This was addressed by creating a series of mutants based on E211S that contained glycine, histidine, or asparagine at position 50 in GABA-AT as well as additional mutations.

The E211S/I50G, E211S/I50G/C77K, and E211S/I50G/C77R mutants were made and tested for transamination and decarboxylation activities. The introduction of either Lys or Arg at position 77 is expected to provide hydrogen bonding/salt bridging interactions with the substrate carboxylate in the stereoelectronically activated position (Scheme 1 and Figure 1). The I50G mutation added to the E211S mutation further reduces k_{cat} for transamination by 190-fold. Remarkably, the additional C77K mutation in the E211S/I50G/C77K mutant leads to the *recovery* of this transamination activity whereas the C77R mutation does not. Only the E211S/I50G/C77K mutant shows significant increases in decarboxylation activity toward both D- and L-glutamate: 9-fold and 5-fold, respectively, compared to wild type (Table 4).

The last strategy employed for introduction of decarboxylation activity into GABA-AT was to orient a polar residue at position 50 such that it is maintained out of the central substrate binding pocket and hydrogen bonds to the substrate carboxylate when it is in the activated position. An examination of the X-ray structure suggested that V80 was the proper location in which to introduce an "anchoring" residue. The choices for residues at postion 50 were histidine and asparagine based on their size and hydrogen bonding abilities. Therefore, the E211S/I50H/V80T, E211S/I50H/V80D, E211S/I50N/V80T, and E211S/I50N/V80D mutants were constructed and analyzed. Of these four mutant enzymes, the E211S/I50H/V80T has transamination activity similar to the parent E211S mutant while the E211S/I50H/V80D has the greatest increase in decarboxylation activity of all the mutants tested: 10-fold for L-glutamate, 6.4-fold for D-glutamate, and 2-fold for α-methylglutamate. Combined with the large reduction in transamination activity that these mutations cause, the increase in decarboxylation activity gives a change in reaction specificity for E211S/I50H/V80D; this mutant actually favors decarboxylation over transamination by 2.7-fold with L-glutamate and 4.3-fold with D-glutamate.

Molecular dynamics calculations were performed on tetramers of the wild-type enzyme with either AOA or D-2-methylglutamate bound as a Schiff base to PLP, and also for the E211S/I50G/C77K and the E211S/V80D/I50H mutants with D-2-methylglutamate bound to gain insight into the low reactivity of the D-2-methylglutamate complexes. The unliganded wild type was used as the initial structure for the D-2-methylglutamate simulations. Crystallographic waters were retained (except those making steric clashes with the ligand). The structures were slowly warmed from 0 to 320 K over 10 ps, followed by equilibration at 320 K for 10 ps, and slow cooling from 320 to 0 K over 10 ps. The final structures were energy minimized for 100 cycles. The overall structures are each very similar to the starting structures, but there are significant active site differences. The wild-type enzyme and E211S/V80D/I50H show steric clashes between the 2-methylglutamate α-carboxylate and either I50 or H50,

while in all four subunits the E211S/I50G/C77K mutant maintains a hydrogen bond/salt bridge between the lysine introduced at position 77 and the D-2-methylglutamate α-carboxylate. The most striking difference between the wild-type AOA structure and all others is in the pyridine nitrogen-D239 interaction. The average distance for the wild-type AOA structure is 3.16 ± 0.05, while it is significantly larger for the D-2-methylglutamate structures with wild type (3.54 ± 0.20), E211S/I50G/C77K (3.39 ± 0.29), and E211S/V80D/I50H (3.62 ± 0.20). This increased pyridine nitrogen-D239 distance due to the relatively poor fit of D-2-methylglutamate in the active site could account for the low reactivity of these complexes.

In summary, it is demonstrated here that V241 in *E. coli* GABA-AT facilitates external aldimine formation with primary amine substrates (e.g. GABA). The role of E211 is shown to be to compensate the positive charge of R398 in the primary amine half-reaction, lowering K_{GABA}, increasing K_{KG}, and increasing the k_{cat} for the overall reaction likely by increasing the rate of the GABA transamination half-reaction. A series of mutants was constructed and analyzed in an attempt to convert GABA-AT into a decarboxylation-dependent aminotransferase, similar to DGD. The largest increase in decarboxylation activity was observed with the E211S/I50H/V80D mutant, which gave 10-fold and 6.4-fold increases with L-and D-glutamate, respectively, and formally converts the reaction specificity of the enzyme from that of a transaminase to a decarboxylase. The moderate success at introducing decarboxylase activity into GABA-AT highlights the greater difficulty of altering the chemistry that an enzyme catalyzes compared to simply altering the substrate that is accepted without changing the catalytic mechanism, as is frequently achieved in studies designed to alter substrate specificity (*24*−*26*).

ACKNOWLEDGMENT

REFERENCES

1. Christen, P., and Metzler, D. E. (1985) *Transaminases*, Wiley, New York.

2. Jansonius, J. N. (1998) Structure, Evolution and Action of Vitamin B6-Dependent Enzymes, *Curr. Opin. Struct. Biol. 8*, 759−69.

3. Mehta, P. K., and Christen, P. (2000) The Molecular Evolution of Pyridoxal-5′-Phosphate-Dependent Enzymes, *Adv. Enzymol. Relat. Areas Mol. Biol. 74*, 129−84.

4. Christen, P., and Mehta, P. K. (2001) From Cofactor to Enzymes. The Molecular Evolution of Pyridoxal-5′-Phosphate-Dependent Enzymes, *Chem. Rec. 1*, 436−47.

5. John, R. A. (1995) Pyridoxal Phosphate-Dependent Enzymes, *Biochim. Biophys. Acta 1248*, 81−96.

6. Percudani, R., and Peracchi, A. (2003) A Genomic Overview of Pyridoxal-Phosphate-Dependent Enzymes, *EMBO Rep. 4*, 850–4.

7. Mehta, P. K., and Christen, P. (1994) Homology of 1-Aminocyclopropane-1-Carboxylate Synthase, 8-Amino-7-Oxononanoate Synthase, 2-Amino-6-Caprolactam Racemase, 2,2-Dialkylglycine Decarboxylase, Glutamate-1-Semialdehyde 2,1-Aminomutase and Isopenicillin-N-Epimerase with Aminotransferases, *Biochem. Biophys. Res. Commun. 198*, 138–43.

8. Toney, M. D., Hohenester, E., Keller, J. W., and Jansonius, J. N. (1995) Structural and Mechanistic Analysis of Two Refined Crystal Structures of the Pyridoxal Phosphate-Dependent Enzyme Dialkylglycine Decarboxylase, *J. Mol. Biol. 245*, 151–79.

9. Hennig, M., Grimm, B., Contestabile, R., John, R. A., and Jansonius, J. N. (1997) Crystal Structure of Glutamate-1-Semialdehyde Aminomutase: An Alpha2-Dimeric Vitamin B6-Dependent Enzyme with Asymmetry in Structure and Active Site Reactivity, *Proc. Natl. Acad. Sci. U.S.A. 94*, 4866–71.

10. Shen, B. W., Hennig, M., Hohenester, E., Jansonius, J. N., and Schirmer, T. (1998) Crystal Structure of Human Recombinant Ornithine Aminotransferase, *J. Mol. Biol. 277*, 81–102.

11. Storici, P., Capitani, G., De Biase, D., Moser, M., John, R. A., Jansonius, J. N., and Schirmer, T. (1999) Crystal Structure of Gaba-Aminotransferase, a Target for Antiepileptic Drug Therapy, *Biochemistry 38*, 8628–34.

12. Liu, W., Peterson, P. E., Carter, R. J., Zhou, X., Langston, J., Fisher, A. J., and Toney, M. D. (2004) Crystal Structures of Unbound and Aminooxyacetate-Bound *Escherichia Coli* Aminobutyrate Aminotransferase, *Biochemistry 43*, 10896–905.

13. Sun, S., Zabinski, R. F., and Toney, M. D. (1998) Reactions of Alternate Substrates Demonstrate Stereoelectronic Control of Reactivity in Dialkylglycine Decarboxylase, *Biochemistry 37*, 3865–75.

14. Dunathan, H. C. (1966) Conformation and Reaction Specificity in Pyridoxal Phosphate Enzymes, *Proc. Natl. Acad. Sci. U.S.A. 55*, 712–6.

15. Aiyar, A., Xiang, Y., and Leis, J. (1996) Site-Directed Mutagenesis Using Overlap Extension Pcr, *Methods Mol. Biol. 57*, 177–91.

16. Arrio-Dupont, M., Coulet, P. R., and Gautheron, D. C. (1985) Coupled Reaction of Immobilized Aspartate Aminotransferase and Malate Dehydrogenase. A Plausible Model for the Cellular Behaviour of These Enzymes, *Biochim. Biophys. Acta 829*, 58–68.

17. Zhou, X., Kay, S., and Toney, M. D. (1998) Coexisting Kinetically Distinguishable Forms of Dialkylglycine Decarboxylase Engendered by Alkali Metal Ions, *Biochemistry 37*, 5761–9.

18. Collaborative Computational Project, N. (1994) The Ccp4 Suite: Programs for Protein Crystallography, *Acta Crystallogr. D50*, 760–763.

19. Segel, I. H. (1993) *Enzyme Kinetics: Behavior and Analysis of Rapid Equilibrium and Steady-State Enzyme Systems*, John Wiley & Sons, New York.

20. Gracia, R., Busquets, M., Gil, M., Cortes, A., and Bozal, J. (1987) A Kinetic Method for Quantification of Aspartate Aminotransferase Isoenzymes, *J. Biochem. Biophys. Methods 15*, 63–9.

21. Quiroga, C., Busquets, M., Cortes, A., and Bozal, J. (1985) Separation and Kinetic Properties of the Molecular Forms of Chicken Liver Cytoplasmic Aspartate Aminotransferase, *Int. J. Biochem. 17*, 1185–90.

22. Orlacchio, A., Campos-Cavieres, M., Pashev, I., and Munn, E. A. (1979) Some Kinetic and Other Properties of the Isoenzymes of Aspartate Aminotransferase Isolated from Sheep Liver, *Biochem. J. 177*, 583–93.

23. Velick, S. F., and Vavra, J. (1962) A Kinetic and Equilibrium Analysis of the Glutamic Oxaloacetate Transaminase Mechanism, *J. Biol. Chem. 237*, 2109–22.

24. Oue, S., Okamoto, A., Yano, T., and Kagamiyama, H. (1999) Redesigning the Substrate Specificity of an Enzyme by Cumulative Effects of the Mutations of Non-Active Site Residues, *J. Biol. Chem. 274*, 2344–9.

25. Yano, T., Oue, S., and Kagamiyama, H. (1998) Directed Evolution of an Aspartate Aminotransferase with New Substrate Specificities, *Proc. Natl. Acad. Sci. U.S.A. 95*, 5511–5.

26. Rothman, S. C., and Kirsch, J. F. (2003) How Does an Enzyme Evolved in Vitro Compare to Naturally Occurring Homologues Possessing the Targeted Function? Tyrosine Aminotransferase from Aspartate Aminotransferase, *J. Mol. Biol. 327*, 593–608.

27. Esnouf, R. M. (1997) An Extensively Modified Version of Molscript That Includes Greatly Enhanced Coloring Capabilities, *J. Mol. Graphics Modell. 15*, 132–4, 112–3.

28. Esnouf, R. M. (1999) Further Additions to Molscript Version 1.4, Including Reading and Contouring of Electron-Density Maps, *Acta Crystallogr., D: Biol. Crystallogr. 55 (Pt 4)*, 938–40.